

The Constraints on CP Violating Phases in models with a dynamical gluino phase

Müge Boz
Hacettepe University, Department of Physics,
06532 Ankara, Turkey

ABSTRACT

We have analyzed the electric dipole moment and the Higgs mass constraints on the supersymmetric model which offers dynamical solutions to the μ and strong CP problems. The trilinear coupling phases, and $\tan\beta - |\mu|$ are strongly correlated, particularly in the low- $\tan\beta$ regime. Certain values of the phases of the trilinear couplings are forbidden, whereas the CP violating phase from the chargino sector is imprisoned to lie near a CP conserving point, by the Higgs mass and electric dipole moment constraints.

1 Introduction

In the standard electroweak theory (SM) the single phase in the CKM matrix, δ_{CKM} , is the unique source for both flavour and CP violations. In the supersymmetric (SUSY) extensions of the standard model, there exist novel sources for both flavour and CP violations coming from the soft supersymmetry breaking mass terms [1]. The new sources of CP violation can be probed via the flavor conserving processes such as the electric dipole moments (EDMs) [2, 3, 4, 5, 6, 7] of the particles, and the Higgs system [8, 9, 10, 11, 12, 13, 14], leading to novel signatures at high-energy colliders [15]. On the other hand, a searching platform for flavour violation is the Higgs-mediated flavour changing processes [16, 17].

The SUSY CP problem is one of the main hierarchy problems that SUSY theories possess. In fact, the EDMs of the neutron and the electron, severely constrain the strength of the CP violation. To evade these constraints, without suppressing the CP violating phases of the theory, several works have been carried out in the existing literature which include choosing the SUSY CP phases very small ($\lesssim \mathcal{O}(10^{-3})$) [2], sparticle masses large [3], arranging for partial cancellations among the different contributions to the EDM [4, 5], and suppressing the phases only in the third generation [18, 19, 20] in the framework of the effective supersymmetry [21].

Clearly, even if the SUSY CP problem is solved, there are still other hierarchy problems in SUSY theories: The strong CP problem whose source is the neutron electric dipole moment exceeding the present bounds by nine orders of magnitude [22], and the μ puzzle, concerning the Higgsino Dirac mass parameter (μ), which follows from the superpotential of the model. A simultaneous solution to both those problems have been shown to exist with a SUSY version [23] of the Peccei-Quinn mechanism, by using a new kind of axion [24, 25], which couples to the gluino rather than to quarks. In this model the invariance of the supersymmetric Lagrangian and all supersymmetry breaking terms under $U(1)_R$ is guaranteed by promoting the ordinary μ parameter to a composite operator involving the gauge singlet \hat{S} with unit R charge. When the scalar component of the singlet develops vacuum expectation value (VEV) around the Peccei-Quinn scale $\sim 10^{11}$ GeV an effective μ parameter $\mu \sim$ a TeV is induced. Besides, the low energy theory is identical to minimal SUSY model with all sources of soft SUSY phases except for the fact that the soft masses are all expressed in terms of the μ parameter through appropriate flavour matrices [23]. The effective Lagrangian of the theory possesses all sources of CP violation through the complex trilinear couplings ($A_{t,b,e}$),

$$A_t = \mu^* k_t, \quad A_b = \mu^* k_b, \quad A_e = \mu^* k_e, \quad (1)$$

the effective μ parameter itself, and the gaugino masses

$$M_1 = k_1 \mu^* , \quad M_2 = k_2 \mu^* , \quad M_3 = |k_3| \mu^* , \quad (2)$$

where $k_{t(b,e)}$ and $k_{1,2,3}$ are the dimensionless complex parameters.

There are other parameters in the model, namely, the squark and the slepton soft masses which assume the form:

$$\begin{aligned} M_Q^2 &= k_Q^2 |\mu|^2 , & M_u^2 &= k_u^2 |\mu|^2 , & M_d^2 &= k_d^2 |\mu|^2 , \\ M_{\tilde{L}}^2 &= k_{\tilde{L}}^2 |\mu|^2 , & M_{\tilde{e}}^2 &= k_{\tilde{e}}^2 |\mu|^2 , \end{aligned} \quad (3)$$

where $k_{\tilde{L},\tilde{e}}$ are real parameters. As suggested by Eqs.(1-3) all soft masses in the theory are fixed in terms of the μ parameter. Therefore, by naturalness, all dimensionless parameters ($|k_i|$) are expected to be of order $\sim \mathcal{O}(1)$.

The main purpose of this work is to study the effects of EDM and Higgs mass constraints on the CP violating phases of the model. To be specific we consider the electron EDM, and analyze the various parameter planes to determine the possible constraints on the μ parameter and the physical phases of the model; that is the phases of stop (A_t), sbottom (A_b), and selectron (A_e) tri-linear couplings:

$$\varphi_{A_t} = Arg[\mu^* k_t] , \quad \varphi_{A_b} = Arg[\mu^* k_b] , \quad \varphi_{A_e} = Arg[\mu^* k_e] , \quad (4)$$

and, of the gaugino masses:

$$\varphi_1 = Arg[\mu^* k_1] , \quad \varphi_2 = Arg[\mu^* k_2]. \quad (5)$$

After having determined the possible constraints on the CP violating phases of the model, from the Higgs mass bound [26, 27] and the eEDM, we will study the dependence of the eEDM on the CP violating phases of the theory, by considering various parameter planes.

The organization of the work is as follows: In Section 2, we study the one and two loop contributions to the eEDM for the model under concern. In Section 3, we carry out the numerical analysis, to study the effects of the EDM and Higgs mass constraints on the CP violating phases of the theory. The results are summarized in Section 4.

2 Electron Electric Dipole Moment

The model under concern does not match to the effective supersymmetry, since all sparticles acquire similar masses. Therefore, in our analysis we take into account of both one and two-loop contributions to eEDM:

$$\left(\frac{d_e}{e}\right) = \left(\frac{d_e}{e}\right)^{1-loop} + \left(\frac{d_e}{e}\right)^{2-loop} . \quad (6)$$

We would like to note that in our presentation we will follow the detailed works of Ibrahim and Nath [4], and Pilaftsis [20]. However, we differ in the sense that in our analysis all the chosen parameters are specific to the gluino-axion model, namely all the soft mass parameters in this theory are fixed in terms of the dynamically-generated μ parameter, whereas the dimensionless parameters involved are naturally of order $\mathcal{O}(1)$ and source the SUSY CP violation.

The main contributions to the one-loop eEDM come from the neutralino, and chargino exchanges, and can be calculated as [4]:

$$\begin{aligned} \left(\frac{d_e}{e}\right)^{1-loop} &= \frac{\alpha}{4\pi s_W^2} \left\{ \sum_{k=1}^2 \sum_{i=1}^4 \text{Im}[\eta_{eik}] \frac{m_{\chi_i^0}}{m_{\tilde{e}_k}^2} B\left(\frac{m_{\chi_i^0}^2}{m_{\tilde{e}_k}^2}\right) \right. \\ &\quad \left. + \frac{m_e}{\sqrt{2} c_\beta m_W m_{\tilde{\nu}_e}^2} \sum_{i=1}^2 m_{\chi_i^+} \text{Im}[U_{i2}^* V_{i1}^*] A\left(\frac{m_{\chi_i^+}^2}{m_{\tilde{\nu}_e}^2}\right) \right\}, \end{aligned} \quad (7)$$

where

$$\begin{aligned} \eta_{eik} &= - \left[\left(t_W \mathcal{N}_{1i} + \mathcal{N}_{2i} \right) \tilde{\mathcal{S}}_{e1k}^* + \frac{m_e}{m_W c_\beta} \mathcal{N}_{3i} \tilde{\mathcal{S}}_{e2k}^* \right] \\ &\quad \times \left[t_W \mathcal{N}_{1i} \tilde{\mathcal{S}}_{e2k} + \frac{m_e}{2m_W c_\beta} \mathcal{N}_{3i} \tilde{\mathcal{S}}_{e1k} \right], \end{aligned} \quad (8)$$

and we set for convenience, $s_W(c_W) = \sin\theta_W(\cos\theta_W)$, $t_W = \tan\theta_W$. In our analysis, the squark (mass)² matrices, expressed in terms of the parameters of the model,

$$\begin{pmatrix} k_{fL}^2 |\mu|^2 + m_f^2 + c_{2\beta}(T_{3f} - Q_f s_W^2) M_Z^2 & m_f \mu (k_f - R_f) \\ m_f \mu^* (k_f - R_f) & k_{fR}^2 |\mu|^2 + m_f^2 + c_{2\beta} Q_f M_Z^2 s_W^2 \end{pmatrix}, \quad (9)$$

can be diagonalized via the unitary rotation:

$$\tilde{\mathcal{S}}_f^\dagger \tilde{M}_f^2 \tilde{\mathcal{S}}_f = \text{diag} \left(m_{\tilde{f}_1}^2, m_{\tilde{f}_2}^2 \right). \quad (10)$$

where $R_f = (t_\beta^{2T_{3f}})^{-1}$, and we set $t_\beta = \tan\beta$, $c_{2\beta} = \cos 2\beta$. Therefore, the eigenstates $(\tilde{e}_1, \tilde{e}_2)$ in (7) can be obtained in analogy with (10) for $f = e$ ($Q_e = -1$, $T_{3e} = -\frac{1}{2}$). Similar analysis can be performed for the sneutrinos, using

$$\tilde{M}_{\nu_e}^2 = \begin{pmatrix} k_{eL}^2 |\mu|^2 + c_{2\beta} T_{3\nu_e} M_Z^2 & 0 \\ 0 & M_G^2 \end{pmatrix}, \quad (11)$$

where $T_{3\nu_e} = \frac{1}{2}$, and M_G is the right-handed sneutrino mass. Moreover, the neutralino and chargino masses in Eq. (7) can be obtained by the following transformations:

$$\mathcal{N}^T M_{\chi^0} \mathcal{N} = \text{diag} \left(m_{\chi_1^0}, \dots, m_{\chi_4^0} \right), \quad (12)$$

$$\mathcal{U}^* M_C \mathcal{V}^{-1} = \text{diag} \left(m_{\chi_1^+}, m_{\chi_2^+} \right). \quad (13)$$

For the two-loop eEDM, the dominant effects originate from the couplings of the Higgs bosons to stop-sbottom quarks, top-bottom quarks and charginos [20]. The Higgs bosons couplings to stop-sbottom quarks can be calculated as [20]:

$$\begin{aligned}
\left(\frac{d_e}{e}\right)_{H_i-\bar{q}}^{2-loop} &= a_0 \alpha m_e \sum_{i=1}^3 \frac{-t_\beta \mathcal{R}_{i3}}{m_{h_i}^2} \left\{ \frac{4}{9} \frac{2m_t^2}{v^2 \Delta_{\bar{t}}} \left[\frac{\text{Im}[\mathcal{Z}_{1t}] \mathcal{R}_{i3}}{s_\beta^2} - \frac{\text{Re}[\mathcal{Z}_{2t}] \mathcal{R}_{i1}}{s_\beta} \right. \right. \\
&+ \left. \frac{\text{Re}[\mathcal{Z}_{3t}] \mathcal{R}_{i2}}{s_\beta} \right] \mathcal{F}_{\bar{t}}^- - \frac{4}{9} \frac{2m_t^2}{v^2} \frac{\mathcal{R}_{2i}}{s_\beta} \mathcal{F}_{\bar{t}}^+ - \frac{1}{9} \frac{2m_b^2}{v^2} \frac{\mathcal{R}_{1i}}{c_\beta} \mathcal{F}_{\bar{b}}^+ \\
&+ \left. \frac{1}{9} \frac{2m_b^2}{v^2 \Delta_{\bar{t}}} \left[\frac{\text{Im}[\mathcal{Z}_{1b}] \mathcal{R}_{i3}}{c_\beta^2} - \frac{\text{Re}[\mathcal{Z}_{2b}] \mathcal{R}_{i2}}{c_\beta} + \frac{\text{Re}[\mathcal{Z}_{3b}] \mathcal{R}_{i1}}{c_\beta} \right] \mathcal{F}_{\bar{b}}^- \right\}, \quad (14)
\end{aligned}$$

where $a_0 = 3/32\pi^3$, and $\Delta_{\bar{q}}$ is the squark splitting ($m_{\bar{q}_2}^2 - m_{\bar{q}_1}^2$). Here, $\mathcal{F}_q^\pm = F(m_{\bar{q}_1}^2, M_A^2) \pm F(m_{\bar{q}_2}^2, M_A^2)$ are the loop functions [20].

In Eq. (14), we define

$$\mathcal{Z}_{1t(b)} = k_{t(b)}, \quad \mathcal{Z}_{2t(b)} = k_{t(b)} - t_\beta^{-1}(t_\beta), \quad \mathcal{Z}_{3t(b)} = |k_{t(b)}|^2 |\mu|^2 - k_{t(b)}^* t_\beta^{-1}(t_\beta), \quad (15)$$

where $k_{t(b)}$ are given by Eq. (4).

Moreover, the radiatively corrected Higgs masses (m_{h_i}) in Eq. (14) can be obtained by the diagonalization of the Higgs mass-squared matrix by the similarity transformation:

$$\mathcal{R} M_H^2 \mathcal{R}^T = \text{diag}(m_{h_1}^2, m_{h_2}^2, m_{h_3}^2), \quad (16)$$

where $\mathcal{R} \mathcal{R}^T = 1$. In our analysis, we define h_3 to be the lightest of all three Higgs bosons, and ρ_3 to be its percentage CP component ($\rho_3 = 100 \times |\mathcal{R}_{13}|^2$) [14, 28]. In Eq. (16), the radiatively corrected (3×3) dimensional Higgs mass-squared matrix has been calculated using the effective potential method, by taking into account the dominant top-stop as well as the bottom-sbottom effects, and the elements of the Higgs mass-squared matrix can be found in [28].

The other contributions to two-loop eEDM come from the Higgs boson couplings to top-bottom quarks [20], and can be expressed in the following form:

$$\begin{aligned}
\left(\frac{d_e}{e}\right)_{H_i-q}^{2-loop} &= b_0 \frac{m_e}{M_W^2} \alpha^2 \sum_{i=1}^3 \left\{ -t_\beta \mathcal{R}_{i3} \left[G_{H_i bt}^{1S} \mathcal{R}_{i1} + G_{H_i bt}^{2S} \mathcal{R}_{i2} + G_{H_i bt}^{3S} \mathcal{R}_{i3} \right] \right. \\
&+ \left. \frac{\mathcal{R}_{i1}}{c_\beta} \left[G_{H_i bt}^{1P} \mathcal{R}_{i1} + G_{H_i bt}^{2P} \mathcal{R}_{i2} + G_{H_i bt}^{3P} \mathcal{R}_{i3} \right] \right\} \quad (17)
\end{aligned}$$

Here, \mathcal{R}_{ij} is defined in Eq. (16), and $b_0 = -3/8\pi^2 s_W^2$, whereas

$$\begin{aligned}
G_{H_i bt}^{1,2S(P)} &= \frac{Q_b^2}{c_\beta} \text{Re}[g_{1,2,bb}^{S(P)}] f(g)(m_b^2, m_{H_i}^2) + \frac{Q_t^2}{s_\beta} \text{Re}[g_{1,2,tt}^{S(P)}] f(g)(m_t^2, m_{H_i}^2), \\
G_{H_i bt}^{3S(P)} &= Q_b^2 \text{Re}[g_{3,bb}^{S(P)}] f(g)(m_b^2, m_{H_i}^2) + Q_t^2 \text{Re}[g_{3,tt}^{S(P)}] f(g)(m_t^2, m_{H_i}^2). \quad (18)
\end{aligned}$$

combine the loop functions $f(g)(m_q^2, m_{H_i}^2)$ with the elements of the coupling coefficients $g_{1,2,3,bb(tt)}^{S(P)}$ [20], for $Q_{t(b)} = \frac{2}{3}(-\frac{1}{3})$.

Finally, the Higgs boson couplings to charginos are given by [20]:

$$\begin{aligned} \left(\frac{d_e}{e}\right)_{H_i-\chi_j^+}^{2-loop} &= -c_0 \frac{m_e \alpha^2}{M_W} \left\{ \sum_{i=1}^3 \sum_{j,k=1,2} \frac{1}{m_{\chi_j^+}} \left[-t_\beta \mathcal{R}_{i3} (\mathcal{C}_{kj}^1 \mathcal{R}_{i1} + \mathcal{C}_{kj}^2 \mathcal{R}_{i2} \right. \right. \\ &\quad \left. \left. + \mathcal{C}_{kj}^3 \mathcal{R}_{i3}) + \frac{\mathcal{R}_{i1}}{c_\beta} (\mathcal{C}'_{kj}^1 \mathcal{R}_{i1} + \mathcal{C}'_{kj}^2 \mathcal{R}_{i2} + \mathcal{C}'_{kj}^3 \mathcal{R}_{i3}) \right] \right\}, \end{aligned} \quad (19)$$

where $c_0 = b_0/3\sqrt{2}$, and \mathcal{C}_{kj} terms represent different combinations of the 2×2 unitary matrices (\mathcal{UV}) , which diagonalize the chargino mass matrix, multiplied by the loop functions $f(g)(m_{\chi_j^+}^2, m_{H_i}^2)$ [20].

3 Numerical Analysis

In the following, we will perform a numerical study to determine the possible constraints on $\tan \beta$, $|\mu|$ and the physical phases of the model. In doing this, we use the present experimental upper bound of the electron EDM [29, 30]:

$$d_e < 4.3 \times 10^{-27} \text{ e.cm}, \quad (20)$$

and impose simultaneously the LEP lower limit on the Higgs mass: $m_{h_3} \gtrsim 115$ GeV (and correspondingly $\tan \beta \gtrsim 3.5$) [26, 27], and all lower bounds on the sparticle masses from direct searches. We would like to note that here we are performing the worst case analysis, that is, we are looking for a Higgs boson which is well inside the existing experimental bounds. Although one can analyze SUSY models with a much lower bound [27], it is important to look for a Higgs boson which has left no trace in LEP data irrespective of the model adopted, SM, or SUSY, or any other extension of SM.

In our analysis, we will particularly concentrate on the lightest Higgs boson, whose CP-odd component as well as its mass are of prime importance in direct Higgs boson searches at high-energy colliders [15]. In fact, we use the lightest Higgs boson as an experimental probe to analyze the dependence of its mass, and CP-odd component on the CP-violating phases of the model, in the parameter space allowed by the EDM constraints.

A convenient way to observe the effects of the EDM constraints, is via the dimensionless quantity:

$$\text{eEDM} = \frac{(d_e/e)^{th}}{(d_e/e)^{exp}}, \quad (21)$$

which measures the fractional enhancement or suppression of the eEDM with respect to its experimental value.

Being a reflecting property of the model, all the soft masses are expressed in terms of the μ parameter, and since the μ parameter is already stabilized to the weak scale as a consequence of naturalness, all dimensionless parameters are expected to be of $O(1)$. One thus notes that when all k parameters are of $O(1)$, all squark soft masses, trilinear couplings, and the gaugino masses scale in exact proportion with the μ parameter.

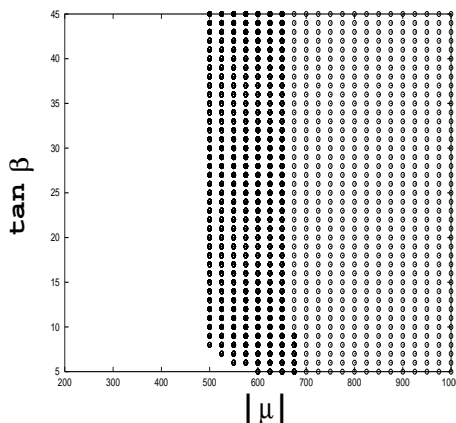


Figure 1: The interdependence of $\tan\beta$ on $|\mu|$, when all the phases are changing from 0 to π , $\tan\beta$ from 5 to 45, and $|\mu|$ from 200 to 1000 GeV.

Our starting point is the general case for which we vary: (i) the phases of stop, sbottom, selectron trilinear couplings (φ_{A_t} , φ_{A_b} , φ_{A_e}), and the phases of the hypercharge gaugino and SU(2) gaugino masses (φ_1 , φ_2) from 0 to π , (ii) $\tan\beta$ from 5 to 45, and (iii) $|\mu|$ from 200 to 1000 GeV. Then, in Fig. 1, we show the dependence of $\tan\beta$ on $|\mu|$. As Fig. 1 suggests, the lower allowed bound on μ , being 500 GeV for $\tan\beta \gtrsim 7$, is pushed to 600 GeV at $\tan\beta \lesssim 7$. For $|\mu| \gtrsim 600$ GeV, all values of $|\mu|$ and $\tan\beta$ are allowed in the full domain. One notes that, the region of the parameter space for which $|\mu| \lesssim 500$ GeV is completely forbidden by the existing constraints on the model, in particular by the experimental constraint on the lightest Higgs boson mass [26], as will be indicated in Fig. 2.

To have a better understanding of the effects of the LEP constraint on the full parameter space, we choose two values of $\tan\beta$, $\tan\beta = 5$, and $\tan\beta = 45$ representing the low and high $\tan\beta$ regimes, respectively, and show the dependence of the lightest Higgs boson mass (m_{h_3}) on $|\mu|$ in Fig. 2, when all the phases change from 0 to π .

As can be seen from Fig. 2 that those portions of the parameter space, corresponding

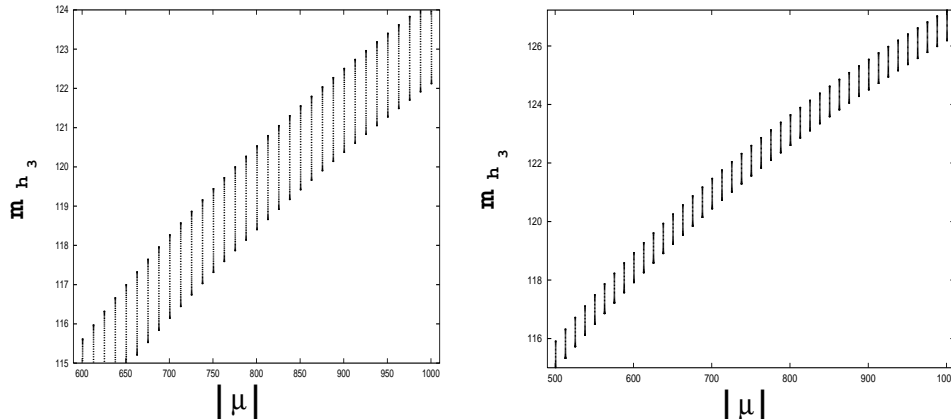


Figure 2: The dependence of the lightest Higgs boson mass (m_{h_3}) on $|\mu|$ when $\tan\beta = 5$ (left panel), and $\tan\beta = 45$ (right panel), when all the phases are changing from 0 to π , and $|\mu|$ from 200 to 1000 GeV.

to $|\mu| \lesssim 600$ GeV for $\tan\beta = 5$, and $|\mu| \lesssim 500$ GeV for $\tan\beta = 45$, are disallowed by the experimental constraint on the lightest Higgs boson mass which requires $m_{h_3} \gtrsim 115$ GeV [26]. A comparative look at both Fig 1, and Fig. 2 suggests that the LEP bound puts important constraints on the parameter space of the model under concern. In general, when all k parameters are naturally of the order of 1, in size, $|\mu|$ can not take values below 500GeV for $\tan\beta \gtrsim 7$, and 600GeV for $5 \lesssim \tan\beta \lesssim 7$. Therefore, constraints from EDM, even if $\tan\beta$ is large, do not exclude a large portion of the parameter space, because of the fact that sparticles are heavy enough to have negligible contributions to the one and two-loop EDMs.

The analyses of Fig. 1 and Fig. 2 give a general idea of the allowed parameter domain in the $\tan\beta - |\mu|$ plane, when all the phases vary in the full range. With this input in mind, to study the possible constraints on the physical phases, we first explore the dependence of φ_{A_t} on $|\mu|$ for low and high values of $\tan\beta$, in Fig. 3.

In Fig. 3, we show the dependence of φ_{A_t} on $|\mu|$ for $\tan\beta = 5$ (left panel), and $\tan\beta = 45$ (right panel), when all the phases are changing from 0 to π . As suggested by the left panel of Fig. 3, at low values of $\tan\beta$, where the two-loop eEDM contributions are negligible, certain values of $|\mu|$ and φ_{A_t} are excluded. For instance, at $\tan\beta = 5$ and $|\mu| = 650$ GeV, the portion of the parameter space for which $\varphi_{A_t} \lesssim \pi/5$ is forbidden. The allowed range of φ_{A_t} gets narrower until $\varphi_{A_t} \sim 7\pi/10$, as μ changes from 650 to 600 GeV. For lower values of μ there is no allowed domain at all. On the other hand, at $\tan\beta = 45$ all points in $\varphi_{A_t} - |\mu|$ plane are allowed for $\mu \gtrsim 500$ GeV, as shown in the right panel of Fig. 3.

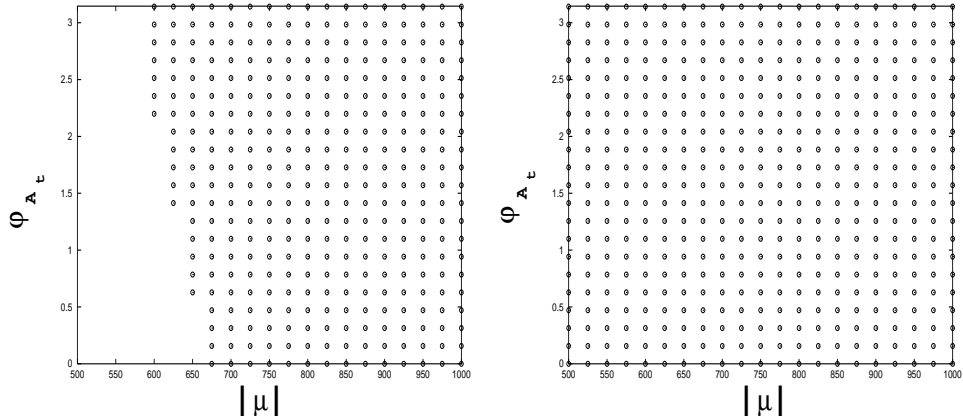


Figure 3: The dependence of φ_{A_t} on $|\mu|$, for $\tan\beta = 5$ (left panel), and $\tan\beta = 45$ (right panel), when all the phases are changing from 0 to π .

A comparative look at both panels of Fig. 3 suggests that, the allowed range of φ_{A_t} and $(\tan\beta, |\mu|)$ become strongly correlated particularly, at low $\tan\beta$. As the allowed range of φ_{A_t} gradually widens (from $7\pi/10$ to $\pi/5$), the lower bound on $|\mu|$ changes from 600GeV to 675GeV, in the low $\tan\beta$ regime (where the main contribution comes from the one-loop eEDM). This constraint on $\varphi_{A_t} - |\mu|$ domain is lifted in the high $\tan\beta$ regime, due to the cancellations between one- and two-loop EDMs.

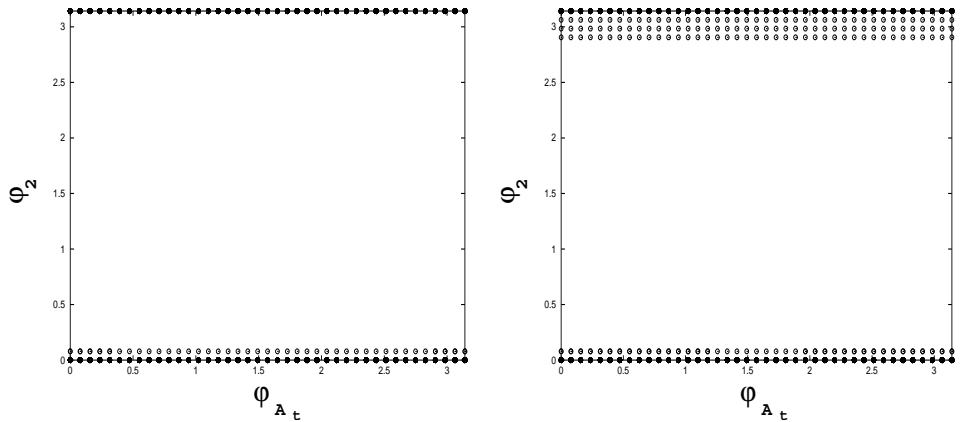


Figure 4: The dependence of φ_2 on φ_{A_t} , for $\mu = 700\text{GeV}$ (left panel), and $\mu = 1000\text{GeV}$ (right panel), at $\tan\beta = 5$, when all the phases changing from 0 to π .

To understand the interdependence of the phase of the $SU(2)$ gaugino mass (φ_2) on φ_{A_t} , and to explore the possible constraints on φ_2 , we first focus on the low- $\tan\beta$ regime, where

φ_{A_t} is quite sensitive to the lower bound on $|\mu|$. We choose two particular values of $|\mu|$ at $\tan\beta = 5$, and in Fig. 4, we show the variation of φ_2 with φ_{A_t} for $|\mu| = 700$ GeV (left panel), and $|\mu| = 1000$ GeV (right panel), when all the phases changing from 0 to π , as in Fig. 3. The left panel of the Fig. 4 suggests that as φ_{A_t} varies in its full range at $|\mu| = 700$ GeV (as has been suggested also by Fig. 3), φ_2 remains in the vicinity of $0 \lesssim \varphi_2 \lesssim \pi/20$. For higher values of φ_2 , no solutions can be found in the parameter space until $\varphi_2 = \pi$. One notes that, $\varphi_{A_t} - \varphi_2$ domain is the similar, for $|\mu| \lesssim 700$ GeV, except for the lower allowed bound of φ_{A_t} which changes from $7\pi/10$ to $\pi/5$ in the $600 \lesssim |\mu| \lesssim 700$ GeV interval.

On the other hand, for higher values of $|\mu|$, for instance at $|\mu| = 1000$ GeV (right panel of Fig. 4), the allowed domain of $\varphi_2 - \varphi_{A_t}$ slightly widens, however, φ_2 still remains in the vicinity of CP-conserving points. The sensitivity of φ_2 becomes stronger in the high- $\tan\beta$ regime, where the two-loop eEDM effects dominate [19, 20].

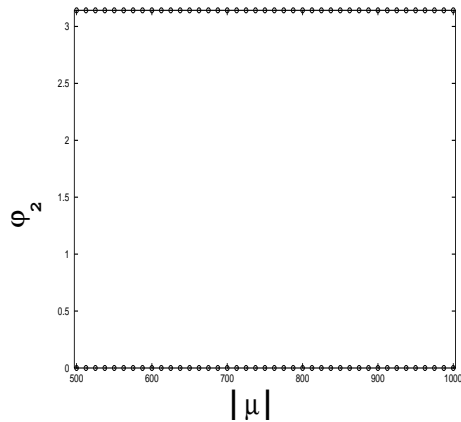


Figure 5: The dependence of φ_2 on $|\mu|$ at $\tan\beta = 45$, when all the phases changing from 0 to π .

For instance, in Fig. 5, we show the dependence of φ_2 on $|\mu|$ at $\tan\beta=45$, when all the phases change from 0 to π , like in all previous cases. It can be seen from Fig. 5 that as $|\mu|$ changes from 500 GeV to 1000 GeV, the phase of the SU(2) gaugino mass is imprisoned to lie at a CP conserving point, for all values of φ_{A_t} , in the high- $\tan\beta$ regime.

A comparative analysis of Fig. 4 and Fig. 5 suggests that the CP violating phase from the chargino sector is required to be in close vicinity of CP conserving points in the low- $\tan\beta$ regime depending on $|\mu|$, whereas it remains stuck completely to CP conserving points in the high- $\tan\beta$, for all values of $|\mu| \gtrsim 500$ GeV. One notes that when all phases are changing from 0 to π , all points in the $\varphi_1 - |\mu|$ plane are allowed in the $600 \lesssim |\mu| \lesssim 1000$ GeV interval, at low- $\tan\beta$ regime ($\tan\beta = 5$). The parameter domain of $\varphi_1 - |\mu|$ plane is similar in the high- $\tan\beta$ regime

($\tan\beta = 45$), but the lower allowed bound of $|\mu|$ becomes 500 GeV for this case.

Since the phase of the SU(2) gaugino mass φ_2 , is sensitive to $\tan\beta$, and $|\mu|$ parameters, and it is required to be in close vicinity of CP conserving points in general, we will take it to be at $\varphi_2 = \pi$, for the rest of the analysis, which we focus on various parameter planes for analyzing the dependence of eEDM on the phases of the trilinear couplings. In doing this, we will vary each of the physical phases in the full $[0, \pi]$ range, setting all the others at the maximal CP violation point.

3.1 $|eEDM|$ versus φ_{A_t}

We show the dependence of $|eEDM|$ on φ_{A_t} in Fig. 6, at $\tan\beta = 5$ (left panel), and $\tan\beta = 45$ (right panel), when $\varphi_1 = \varphi_{A_b} = \varphi_{A_e} = \varphi_{1,b,e} = \pi/2$, and φ_{A_t} changes in the $[0, \pi]$ interval.

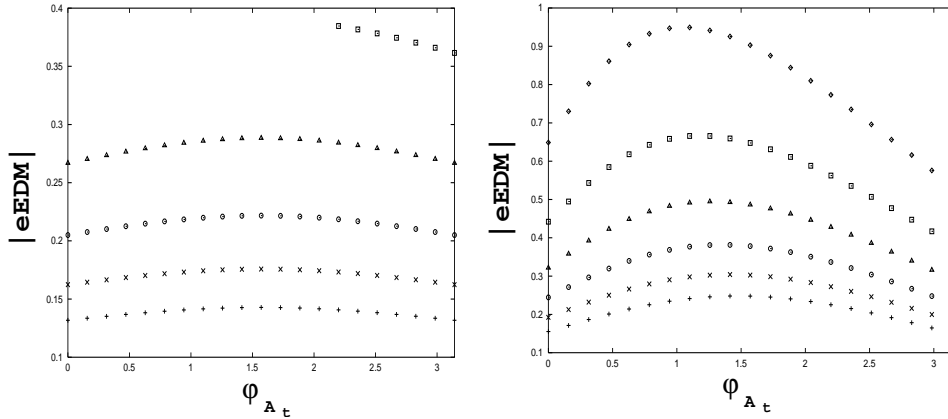


Figure 6: The dependence of $|eEDM|$ on φ_{A_t} at $\tan\beta = 5$ (left panel), and $\tan\beta = 45$ (right panel), when $\varphi_{1,b,e} = \pi/2$. In both panels, those portions of the parameter space presented by the curves “ \square ”, “ \triangle ”, “ \circ ”, “ \times ”, belong to 600, 700, 800, 900, 1000GeV values of $|\mu|$, respectively, whereas “ \diamond ” corresponds to $|\mu| = 500$ GeV in the right panel.

In both panels of Fig. 6, the various curves shown by “ \square ”, “ \triangle ”, “ \circ ”, “ \times ”, “ $+$ ” belong to 600, 700, 800, 900, 1000GeV values of $|\mu|$, respectively, whereas “ \diamond ” corresponds to $|\mu| = 500$ GeV in the right panel. As the left panel of the Figure suggests, in the low- $\tan\beta$ regime (where the two-loop EDM contributions are small), $|eEDM|$ maximally extends to ~ 0.4 at $\mu = 600$ GeV (“ \square ”), and at $\varphi_{A_t} \gtrsim 7\pi/10$. The remaining portion of the parameter space ($\varphi_{A_t} \lesssim 7\pi/10$) is discarded by the existing constraints on the model (see, Fig. 3). On the other hand, as μ gets larger values, $|eEDM|$ decreases. For instance, when $|\mu| = 1000$ GeV (“ $+$ ”), the maximal value of $|eEDM|$ does not exceed ~ 0.15 in the low- $\tan\beta$ regime (left panel). For the high- $\tan\beta$ regime (right panel), the upper bound of the $|eEDM|$ increases, whereas the allowed range of

$|\mu|$ widens, as compared to $\tan\beta = 5$ case. For instance, as φ_{A_t} ranges in the full $[0, \pi]$ interval, the maximal value of $|eEDM|$ occurs at $|\mu| = 500\text{GeV}$ ("◇") when $\tan\beta = 45$. A comparative look at both panels of Fig. 6 suggests that $|eEDM|$ grows with $\tan\beta$, and it approaches to the upper bound, particularly in the high- $\tan\beta$ regime, since the two-loop EDM contribution grows with $\tan\beta$.

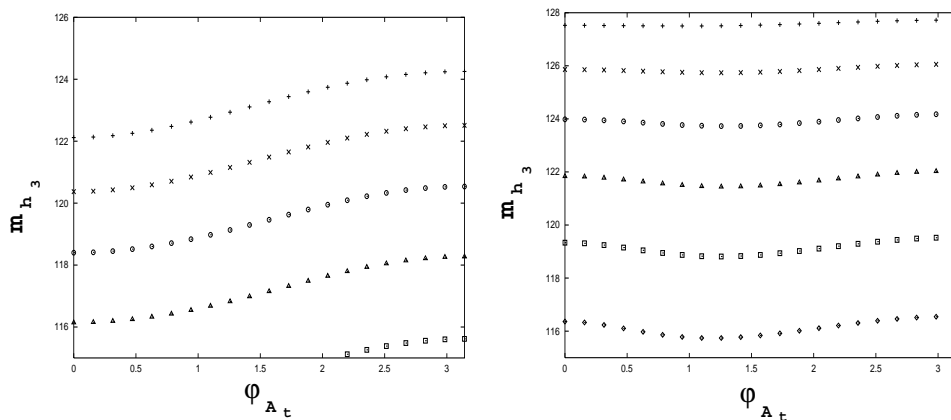


Figure 7: The dependence of mass of the lightest Higgs boson (m_{h_3}) on φ_{A_t} at $\tan\beta = 5$ (left panel), and $\tan\beta = 45$ (right panel), when $\varphi_{1,b,e} = \pi/2$. In both panels, “□”, “△”, “○”, “×”, “+”, represent 600, 700, 800, 900, 1000 GeV values of $|\mu|$, respectively, whereas “◇” corresponds to $|\mu| = 500\text{GeV}$ in the right panel.

In Fig. 7, we show the variation of the mass of the lightest Higgs boson (m_{h_3}) with φ_{A_t} , at $\tan\beta = 5$ (left panel), and $\tan\beta = 45$ (right panel), when $\varphi_{1,b,e} = \pi/2$. As in Fig. 6, in both panels of Fig. 7, the curves shown by “□”, “△”, “○”, “×”, “+”, present 600, 700, 800, 900, 1000 GeV, values of $|\mu|$, respectively, whereas “◇” belongs to $|\mu| = 500\text{GeV}$ in the right panel. It can be seen from the left panel that, being $\lesssim 116\text{GeV}$ at the lower bound ($|\mu| = 600\text{GeV}$, “□”), m_{h_3} maximally extends to $\sim 124\text{GeV}$ when $|\mu| = 1000\text{GeV}$ (“+”), in the low $\tan\beta$ regime. Therefore, as $|\mu|$ gets larger values, m_{h_3} increases, which remains true also in the high- $\tan\beta$ regime (right panel). A comparative look at both panels of Fig. 7 suggests that m_{h_3} is much more sensitive to the variations in φ_{A_t} at $\tan\beta = 5$ (left panel), than that of $\tan\beta = 45$ (right panel), since the radiative corrections depend strongly on the stop splitting at low- $\tan\beta$ regime. On the other hand, the dependence of m_{h_3} on φ_{A_t} weakens in passing from the low $\tan\beta$ regime to higher, since the radiative corrections to m_{h_3} which are sensitive to the variations in φ_{A_t} are suppressed in the high- $\tan\beta$ regime [14]. One notes that this is the region of the parameter space in which $0.1 \lesssim |eEDM| \lesssim 0.4$ for $\tan\beta = 5$, and $0.1 \lesssim |eEDM| \lesssim 0.98$ for $\tan\beta = 45$, as has been suggested by Fig. 6.

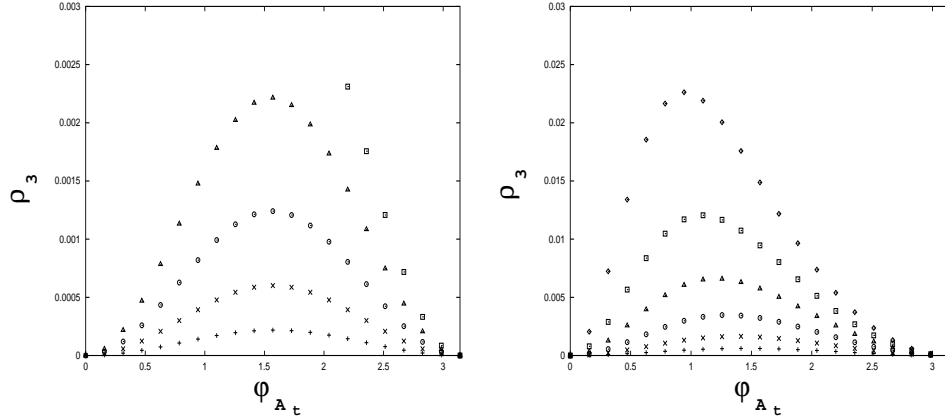


Figure 8: The dependence of the CP-odd component (ρ_3) of the lightest Higgs boson on φ_{A_t} at $\tan\beta = 5$ (left panel), and $\tan\beta = 45$ (right panel), when $\varphi_{1,b,e} = \pi/2$, and $|\mu| = 600$ ("□"), 700 ("△"), 800 ("○"), 900 ("×"), 1000 ("+") GeV (in both panels), and $|\mu| = 500$ GeV ("◇", right panel)

In Fig. 8, we show the variation of the CP-odd component (ρ_3) of the lightest Higgs boson with φ_{A_t} , for $\tan\beta = 5$ (left panel), and $\tan\beta = 45$ (right panel), at $\varphi_{1,b,e} = \pi/2$, when $|\mu| = 600$ ("□"), 700 ("△"), 800 ("○"), 900 ("×"), 1000 ("+") GeV (in both panels), and $|\mu| = 500$ GeV ("◇", right panel). As both panels of the Figure suggest, higher the $|\mu|$, smaller the ρ_3 . Such kind of $\rho_3 - |\mu|$ interdependence is expected, since we particularly focus on the region of the parameter space for which the scale dependence is sufficiently suppressed ($1000 \lesssim Q \lesssim 1200$) [28], and we set, for convenience, $Q = 1200$ GeV. The properties of various renormalization scales, changing from top mass to TeV scale, and particularly their influences on $\rho_3 - \mu$ plane has been studied in Ref. [28].

The dependence of m_{h_3} , and ρ_3 on φ_{A_t} in the parameter space allowed by the EDM constraints shows that, being quite sensitive to the variations in φ_{A_t} , m_{h_3} maximally reaches to ~ 128 GeV when $\mu = 1000$ GeV, and $\tan\beta = 45$. On the other hand, ρ_3 remains below $\sim 0.3\%$ though it grows by more than an order of magnitude as $\tan\beta$ changes from 5 to 45. This is similar to constraints found for MSSM Higgs sector [9].

3.2 $|eEDM|$ versus φ_{A_e}

In Fig. 9, we show the variation of $|eEDM|$ with the selectron trilinear coupling (φ_{A_e}) at $\tan\beta = 5$ (left panel), and $\tan\beta = 45$ (right panel), when $\varphi_1 = \varphi_{A_t} = \varphi_{A_b} = \varphi_{1,t,b} = \pi/2$, and φ_{A_e} changes in the $[0, \pi]$ interval.

In the figure, 500, 600, 700, 800, 900, 1000 GeV, values of $|\mu|$ are presented by the curves

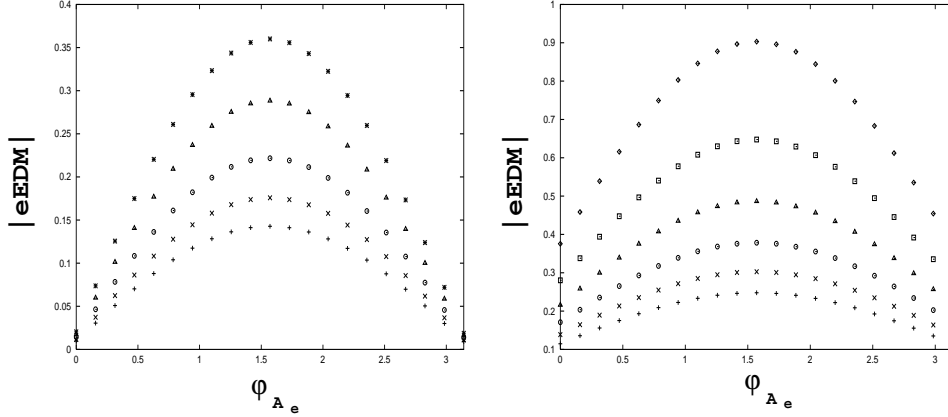


Figure 9: The dependence of $|eEDM|$ on φ_{A_e} at $\tan\beta = 5$ (left panel), and $\tan\beta = 45$ (right panel), when $\varphi_{1,t,b} = \pi/2$. In the figure, 500, 600, 700, 800, 900, 1000 GeV values of $|\mu|$ are presented by the curves "□", "◇", "△", "○", "×", "+", whereas $|\mu| = 625$ GeV ("*") is the lower allowed bound at $\tan\beta = 5$ (left panel)

"□", "◇", "△", "○", "×", "+", whereas "*" (left panel), corresponds to $|\mu| = 625$ GeV. One notes that, at $\tan\beta = 5$ (left panel), the region of the parameter space for which $|\mu| \lesssim 625$ GeV is forbidden by the existing constraints on the model. Indeed, remembering the $\varphi_{A_t} - |\mu|$ domain in Fig. 3 for instance, it can be seen that the lower allowed bound on $|\mu|$ is pushed from 600 to 625 GeV for $\varphi_{A_t} \gtrsim \pi/2$ at $\tan\beta = 5$. Such a constraint is lifted in the high- $\tan\beta$ regime, and all points in the $\varphi_{A_t} - \varphi_{A_e}$ are allowed for $|\mu| \gtrsim 500$ GeV. As both panels of the Figure suggest, the variation of φ_{A_e} around $\varphi_{A_e} = \pi/2$ differs from those at $\varphi_{A_e} = 0$, and $\varphi_{A_e} = \pi$. That is, increasing with φ_{A_e} in the $[0, \pi/2]$ interval, the maximal value of $|eEDM|$ occurs at $\varphi_{A_e} = \pi/2$. Then, it gradually decreases in the $[\pi/2, \pi]$ interval.

3.3 $|eEDM|$ versus $(\tan\beta, |\mu|)$

Finally, in Fig. 10, we have shown the dependence of $|EDM|$ on $|\mu|$, when the physical phases of the model are chosen as: $\varphi_1 = \varphi_{A_t} = \varphi_{A_b} = \varphi_{A_e} = \varphi_{1tbe} = \pi/2$, whereas $\varphi_2 = \pi$, like all the previous cases.

In Fig. 10, we have chosen various values of $\tan\beta$, which are represented by the curves: $\tan\beta = 5$ ("+"), $\tan\beta = 15$ ("×"), $\tan\beta = 25$ ("○"), $\tan\beta = 35$ ("□"), $\tan\beta = 45$ ("△"). As Fig. 10 suggests, when $\varphi_{1tbe} \rightsquigarrow \pi/2$, being ~ 0.35 for $\tan\beta = 5$, the maximal value of $|eEDM|$ reaches beyond ~ 0.9 for $\tan\beta = 45$, when $\varphi_{1tbe} \rightsquigarrow \pi/2$. Therefore, as has been mentioned in the previous cases (for instance, Fig. 5), the general tendency of $|eEDM|$ is such that it grows with $\tan\beta$. However, the dependence of $|eEDM|$ on $|\mu|$ differs from that of $\tan\beta$ in the sense

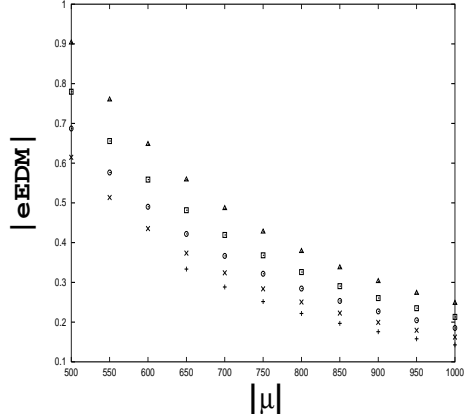


Figure 10: The dependence of $|eEDM|$ on $|\mu|$, at $\tan \beta = 5$ ("+"), 15 ("×"), 25 ("o"), 35 ("□"), 45 ("△"), when $\varphi_{1tbe} = \pi/2$.

that $|eEDM|$ decreases as $|\mu|$ gets higher values.

In Fig. 11, which supplements Fig. 10, the variation of $|eEDM|$ with $\tan \beta$ is shown, when $\varphi_{1tbe} \rightsquigarrow \pi/2$. Here, the curves shown by "+", "o", "□", "△", "◇" represent $\mu = 500, 600, 700, 800, 900, \text{ and } 1000$ GeV. values of $|\mu|$. As the Figure suggests, when $\tan \beta = 45$, $|eEDM|$ occurs at ~ 0.2 , at $\mu = 1000$ GeV. Increasing gradually, it reaches far below ~ 0.5 at $\mu = 700$ GeV, and finally when $\mu = 500$ GeV, $|eEDM|$ approaches to the upper bound.

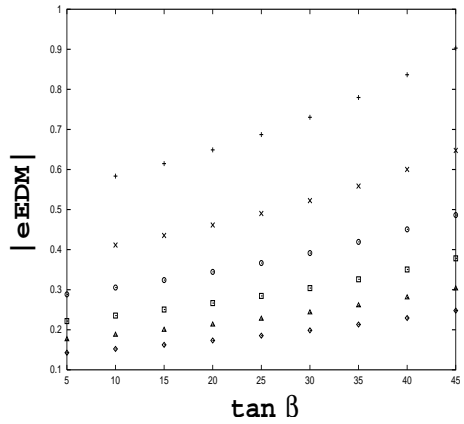


Figure 11: The dependence of $|eEDM|$ on $\tan \beta$ for various values of $|\mu|$ when $\varphi_{1tbe} = \pi/2$. Here, $|\mu| = 500$ ("+"), 600 ("×"), 700 ("o"), 800 ("□"), 900 ("△"), 1000 ("◇") GeV.

Therefore, similar to observations made for the former case (Fig. 10), one notices that, as $|\mu|$ gets larger values, $|eEDM|$ decreases. The reason for that is, as has been suggested by Eqs.

(1-3), all the soft mass parameters of the model are expressed in terms of the μ parameter, and clearly, as $|\mu|$ gets larger values, the sparticle masses increase.

Taking into account of the fact that eEDM decreases, as the sparticle masses increase in general, such kind of $|eEDM| - |\mu|$ dependence is expected (higher the $|\mu|$ parameter, heavier the sparticle masses, and smaller the SUSY contributions to the $|eEDM|$).

Before concluding, we would like to note that, although we did not show explicitly, the branching ratio $B \rightarrow X_s \gamma$ remains within the bounds. The main reason for having agreement with $B \rightarrow X_s \gamma$ constraints is that generally $\mu \gtrsim 500\text{GeV}$, and the pseudoscalar and charged Higgs bosons, like the sfermions themselves, are heavy. Therefore, within this spectrum, non-standard contributions to $B \rightarrow X_s \gamma$ are suppressed [31, 32, 33, 34, 35].

4 Conclusion

We have analyzed the EDM and Higgs mass constraints on the SUSY model which solve the strong CP problem via the dynamical phase of the gluino mass [23]. The model expresses all soft breaking masses in terms of the dynamically-generated μ parameter where the dimensionless parameters involved are naturally of order $\mathcal{O}(1)$ and source the SUSY CP violation.

Our general discussion followed by the numerical estimates for various parameter planes show that: when all the phases are changing from 0 to π , (i) $|\mu|$ is forbidden to take values typically below 500 GeV by the LEP constraint on the lightest Higgs mass. This is an interesting constraint which has been seen to weaken EDM constraints due to the heaviness of the superpartners. (ii) in contrast to the constrained minimal model, or unconstrained low energy minimal supersymmetric model, certain values of the trilinear coupling phases are disallowed due to both the electric dipole moment and the Higgs mass constraints. (iii) as in the minimal supersymmetric model, in general, the CP violating phase from the chargino sector (φ_2) is required to be in close vicinity of a CP-conserving point.

5 Acknowledgements

This work was partially supported by the Scientific and Technical Research Council of Turkey (TÜBİTAK) under the project, No:TBAG-2002(100T108).

The author also thanks Durmuş Demir for useful e-mail exchange.

References

- [1] M. Dugan, B. Grinstein and L. J. Hall, Nucl. Phys. B **255**, 413 (1985).
- [2] J. R. Ellis, S. Ferrara and D. V. Nanopoulos, Phys. Lett. B **114**, 231 (1982); J. Polchinski and M. B. Wise, Phys. Lett. B **125**, 393 (1983); T. Falk, K. A. Olive and M. Srednicki, Phys. Lett. B **354**, 99 (1995) [arXiv:hep-ph/9502401]; S. Pokorski, J. Rosiek and C. A. Savoy, Nucl. Phys. B **570**, 81 (2000) [arXiv:hep-ph/9906206]; E. Accomando, R. Arnowitt and B. Dutta, Phys. Rev. D **61**, 115003 (2000) [arXiv:hep-ph/9907446].
- [3] P. Nath, Phys. Rev. Lett. **66**, 2565 (1991); Y. Kizukuri and N. Oshimo, Phys. Rev. D **45**, 1806 (1992).
- [4] T. Ibrahim and P. Nath, Phys. Lett. B **418**, 98 (1998) [arXiv:hep-ph/9707409]; T. Ibrahim and P. Nath, Phys. Rev. D **57**, 478 (1998) [Erratum-ibid. D **58**, 019901 (1998 ERRAT,D60,079903.1999 ERRAT,D60,119901.1999)] [arXiv:hep-ph/9708456].
- [5] T. Falk and K. A. Olive, Phys. Lett. B **439**, 71 (1998) [arXiv:hep-ph/9806236]; M. Brhlik, G. J. Good and G. L. Kane, Phys. Rev. D **59**, 115004 (1999) [arXiv:hep-ph/9810457]; M. Brhlik, L. L. Everett, G. L. Kane and J. Lykken, Phys. Rev. D **62**, 035005 (2000) [arXiv:hep-ph/9908326].
- [6] T. Ibrahim and P. Nath, Phys. Rev. D **58**, 111301 (1998) [Erratum-ibid. D **60**, 099902 (1999)] [arXiv:hep-ph/9807501]; T. Ibrahim and P. Nath, Phys. Rev. D **61**, 093004 (2000) [arXiv:hep-ph/9910553].
- [7] D. A. Demir, M. Pospelov and A. Ritz, Phys. Rev. D **67**, 015007 (2003) [arXiv:hep-ph/0208257].
- [8] A. Pilaftsis, Phys. Lett. B **435**, 88 (1998) [arXiv:hep-ph/9805373]; Phys. Rev. D **58**, 096010 (1998) [arXiv:hep-ph/9803297]; A. Pilaftsis and C. E. Wagner, Nucl. Phys. B **553**, 3 (1999) [arXiv:hep-ph/9902371].
- [9] D. A. Demir, Phys. Rev. D **60**, 055006 (1999) [arXiv:hep-ph/9901389]; Nucl. Phys. Proc. Suppl. **81**, 224 (2000) [arXiv:hep-ph/9907279].
- [10] S. Y. Choi, M. Drees and J. S. Lee, Phys. Lett. B **481**, 57 (2000) [arXiv:hep-ph/0002287].
- [11] M. Carena, J. R. Ellis, A. Pilaftsis and C. E. Wagner, Nucl. Phys. B **586**, 92 (2000) [arXiv:hep-ph/0003180].

- [12] T. Ibrahim and P. Nath, Phys. Rev. D **63**, 035009 (2001) [arXiv:hep-ph/0008237];
T. Ibrahim, Phys. Rev. D **64**, 035009 (2001) [arXiv:hep-ph/0102218].
- [13] S. W. Ham, S. K. Oh, E. J. Yoo and H. K. Lee, J. Phys. G **27**, 1 (2001).
- [14] M. Boz, Mod. Phys. Lett. A **17**, 215 (2002) [arXiv:hep-ph/0008052].
- [15] M. Carena, J. R. Ellis, A. Pilaftsis and C. E. Wagner, Phys. Lett. B **495**, 155 (2000) [arXiv:hep-ph/0009212]; M. Carena, J. R. Ellis, A. Pilaftsis and C. E. Wagner, Nucl. Phys. B **625**, 345 (2002) [arXiv:hep-ph/0111245]; M. Carena, J. Ellis, S. Mrenna, A. Pilaftsis and C. E. Wagner, arXiv:hep-ph/0211467.
- [16] M. Boz and N. K. Pak, Phys. Rev. D **65**, 075014 (2002).
- [17] T. Ibrahim and P. Nath, Phys. Rev. D **67**, 016005 (2003) [arXiv:hep-ph/0208142]; A. Dedes and A. Pilaftsis, Phys. Rev. D **67**, 015012 (2003) [arXiv:hep-ph/0209306]; D. A. Demir, Phys. Lett. B **571**, 193 (2003) [arXiv:hep-ph/0303249].
- [18] D. A. Demir and M. B. Voloshin, Phys. Rev. D **63**, 115011 (2001) [arXiv:hep-ph/0012123].
- [19] D. Chang, W. Y. Keung and A. Pilaftsis, Phys. Rev. Lett. **82**, 900 (1999) [Erratum-ibid. **83**, 3972 (1999)] [arXiv:hep-ph/9811202]. A. Pilaftsis, Phys. Lett. B **471**, 174 (1999) [arXiv:hep-ph/9909485]; D. Chang, W. F. Chang and W. Y. Keung, Phys. Lett. B **478**, 239 (2000) [arXiv:hep-ph/9910465].
- [20] A. Pilaftsis, Nucl. Phys. B **644**, 263 (2002) [arXiv:hep-ph/0207277].
- [21] S. Dimopoulos and G. F. Giudice, Phys. Lett. B **357** (1995) 573 [arXiv:hep-ph/9507282]; P. Binetruy and E. Dudas, Phys. Lett. B **389** (1996) 503 [arXiv:hep-th/9607172]; G. R. Dvali and A. Pomarol, Phys. Rev. Lett. **77** (1996) 3728 [arXiv:hep-ph/9607383]; A. G. Cohen, D. B. Kaplan and A. E. Nelson, Phys. Lett. B **388** (1996) 588 [arXiv:hep-ph/9607394].
- [22] P. G. Harris *et al.*, Phys. Rev. Lett. **82**, 904 (1999).
- [23] D. A. Demir and E. Ma, Phys. Rev. D **62**, 111901 (2000) [arXiv:hep-ph/0004148]; D. A. Demir, E. Ma and U. Sarkar, J. Phys. G **26**, L117 (2000) [arXiv:hep-ph/0005288]; D. A. Demir and E. Ma, J. Phys. G **27**, L87 (2001) [arXiv:hep-ph/0101185].
- [24] R. D. Peccei and H. R. Quinn, Phys. Rev. Lett. **38**, 1440 (1977).

- [25] J. E. Kim, Phys. Rev. Lett. **43**, 103 (1979); M. A. Shifman, A. I. Vainshtein and V. I. Zakharov, Nucl. Phys. B **166**, 493 (1980); M. Dine, W. Fischler and M. Srednicki, Phys. Lett. B **104**, 199 (1981).
- [26] LEPC, Nov 3, 2000, P Igo-Kemenes,
<http://www.cern.ch/LEPHIGGS/talks/index.html>.
- [27] The LEP Higgs Working Group for Higgs boson searches, arXiv:hep-ex/0107029; arXiv:hep-ex/0107030; ALEPH,DELPHI,L3 and OPAL Collaborations, The LEP Higgs Working Group for Higgs Boson Searches, LHWG Note/2001-04 (2001), LHWG Note/2002-01 (2002), <http://www.cern.ch/LEPHIGGS/www/Welcome.html>.
- [28] M. Boz, J. Phys. G **28**, 2377 (2002) [arXiv:hep-ph/0207050].
- [29] E. D. Commins, S. B. Ross, D. DeMille and B. C. Regan, Phys. Rev. A **50**, 2960 (1994).
- [30] K. Abdullah, C. Carlberg, E. D. Commins, H. Gould and S. B. Ross, Phys. Rev. Lett. **65**, 2347 (1990).
- [31] S. Bertolini, F. Borzumati, A. Masiero and G. Ridolfi, Nucl. Phys. B **353**, 591 (1991); F. M. Borzumati, Z. Phys. C **63**, 291 (1994) [arXiv:hep-ph/9310212].
- [32] A. L. Kagan and M. Neubert, Phys. Rev. D **58**, 094012 (1998) [arXiv:hep-ph/9803368]; Eur. Phys. J. C **7**, 5 (1999) [arXiv:hep-ph/9805303].
- [33] G. Degrossi, P. Gambino and G. F. Giudice, JHEP **0012**, 009 (2000) [arXiv:hep-ph/0009337]; M. Carena, D. Garcia, U. Nierste and C. E. Wagner, Phys. Lett. B **499**, 141 (2001) [arXiv:hep-ph/0010003].
- [34] D. A. Demir and K. A. Olive, Phys. Rev. D **65**, 034007 (2002) [arXiv:hep-ph/0107329]; M. Boz and N. K. Pak, Phys. Lett. B **531**, 119 (2002) [arXiv:hep-ph/0201199].
- [35] A. L. Kagan, AIP Conf. Proc. **618**, 310 (2002) [arXiv:hep-ph/0201313]; M. Neubert, arXiv:hep-ph/0212360.